Water interaction with dielectric surface: A combined *ab initio* modeling and experimental study

Cite as: Phys. Fluids **33**, 042012 (2021); https://doi.org/10.1063/5.0046587
Submitted: 04 February 2021 . Accepted: 06 April 2021 . Published Online: 28 April 2021

Vitaliy Yurkiv, Jingwei Wu, Subhayan Halder, Rafael Granda, Abhilash Sankaran, Alexander L. Yarin, and Farzad Mashayek

Physics of Fluids ARTICLE scitation.org/journal/phf

Water interaction with dielectric surface: A combined *ab initio* modeling and experimental study

Cite as: Phys. Fluids **33**, 042012 (2021); doi: 10.1063/5.0046587
Submitted: 4 February 2021 · Accepted: 6 April 2021 ·
Published Online: 28 April 2021

Vitaliy Yurkiv,[a] Jingwei Wu, Subhayan Halder, Rafael Granda, Abhilash Sankaran, Alexander L. Yarin, and Farzad Mashayek

AFFILIATIONS

Department of Mechanical and Industrial Engineering, University of Illinois at Chicago, Chicago, Illinois 60607, USA

[a]Author to whom correspondence should be addressed: vyurkiv@uic.edu

ABSTRACT

A combined *ab initio* modeling and experimental study of water adsorption on a dry hydrophobic dielectric surface is presented. This is an important phenomenon for controlled droplet deposition in various technological applications. The *ab initio* density functional theory calculations are performed to reveal the dominant water adsorption sites, energetics, and the electron density profile on Teflon and parafilm surfaces. Several surface states such as stretched, nondefective, and defective are considered for water adsorption studies. It is revealed that stretching of nondefective surface leads to weaker water adsorption compared to an unstretched surface. Accordingly, such stretching makes the surface more hydrophobic as revealed by the electron density profile. The introduction of random defects into Teflon and parafilm surfaces results in an increase in water adsorption energy leading, in some cases, to practically hydrophilic interactions. These findings are in good agreement with the present measurements of static contact angle on prestretched Teflon and parafilm samples, where stretching not only elongates interatomic bonds but also changes the surface roughness. Thus, the present combined modeling and experimental study allows for a mechanistic interpretation of the reasons behind the change of wettability of dry hydrophobic surfaces.

I. INTRODUCTION

Controlled droplet deposition onto a dry surface is important for various technologies such as spray cooling and spray painting, pesticide deposition, inkjet printing, coating, etc.[1–6] In the last two decades, droplet impact onto dry hydrophobic surfaces has received significant attention of the research and industrial communities and several distinct droplet impact patterns have been revealed, such as receding breakup, prompt and corona splashing, partial rebound, and complete rebound in addition to deposition.[2–9] It has been discovered that the flow pattern depends upon the droplet impact velocity, liquid properties, surface wettability and roughness, and the receding contact angle of the droplet.[4,8–10] Enhanced understanding of droplet rebound and splashing can improve the effectiveness of coating and painting applications while decreasing the spraying costs due to material loss. In particular, the state of the impacting surface and the static contact angle is of imperative importance, albeit least understood thus far. During the prespraying treatment and preparation of surfaces, a variety of dislocations, kinks, steps, and distortions can be formed, and it is difficult to study experimentally their effect on droplet impact and deposition. The physicochemical influence of the state of surface on droplet impact lays at the subnanometer level, where water molecules interact with the surface atoms of the substrate.[11,12]

The objective of this work is to investigate water interactions with Teflon and parafilm surfaces at the atomic level using the density functional theory (DFT). Because the structure and properties of Teflon and parafilm surface layers significantly depend on the prespraying surface preparation, the two most common subsystems with ordered and amorphous surfaces are considered in this work. Among several existing techniques,[13–15] the DFT is the most powerful and widely accepted approach to study interfacial systems at the atomic level. Solving the governing equations *ab initio*, the DFT provides a valuable tool for predicting water adsorption energy and structures at the interfaces. The knowledge of atomic-level interactions of water and hydrophobic surfaces is important for a better understanding of the fundamental level yielding better predictive capabilities contributing to rejuvenation of modern spray technologies.

In recent years, there has been a tremendous increase in the number of studies dedicated to interface and contact angle

investigations employing a variety of methods;[12,16–20] however, only a few of them deal with the water adsorption contact angle estimation, vapor–liquid interface and electron density analysis. A series of outstanding works dedicated to a vapor–liquid interface study have been published by Gross and colleagues[21–24] using the DFT method. Sauer *et al.*[22] have reported the prediction of a contact angle of sessile droplets using the classical DFT based on the perturbed-chain polar statistical associating fluid theory (PCP-SAFT) equation-of-state. They demonstrated that DFT is capable of predicting contact angles of real substances in good agreement with experimental data. In addition, they showed that the DFT predictions are in good agreement with the Monte Carlo (MC) molecular simulations in terms of density profile and static contact angle.

Thiele's and Archer's groups have published results on liquid droplets on surfaces[13,25,26] using similar DFT approaches. Hughes *et al.*[26] have developed a microscopic DFT-based method for calculating the binding energies of different state points and interaction potentials between the surface and the liquid. The DFT-based results were used in the mesoscopic interface free energy model to calculate the height profile of liquid droplets on a surface. They showed that mesoscopic liquid height profiles are very similar in shape to the profiles obtained in the framework of the DFT.

Teflon (polytetrafluoroethylene) has been the subject of several atomistic studies, which employed the DFT and the molecular dynamics (MD) models. Brownell *et al.* have studied deformation and mechanical failures of single chain and bulk Teflon using the MD.[27] The ReaxFF simulations have been used to derive the coarse-grain potential parameters to study the microscale mechanical properties of Teflon. The most optimal molecular structures of Teflon were identified and it was shown that temperature has a pronounced effect on the maximum strength of a single Teflon chain. It was also shown that the elastic modulus is dependent on the chain length.

The present paper is structured as follows. First, the theoretical and experimental methodologies are described. Then, the results on water adsorption on Teflon surfaces are presented followed by the results for paraffin surfaces. At the end, conclusions are drawn.

II. METHODOLOGY

In the present work, water interaction with Teflon and parafilm surfaces is studied using the DFT and compared to the experimental measurements of static contact angles. Different states of surface and adsorbate structures are considered, and the electron densities are analyzed as sketched in the zoomed-in image in Fig. 1.

DFT methodology. In this work, we use the DFT calculations as implemented in the Vienna *Ab Initio* Simulations Package (VASP) code, which employs the generalized-gradient approximation (GGA) using the optB86b-vdW functional to account for the exchange–correlation effects and van der Waals energy.[28,29] For a system with an odd number of electrons, unrestricted spin-polarized calculations and for a system with an even number of electrons, nonspin-polarized calculations are performed. For all calculations, a cutoff energy of 550 eV is used. All structural optimizations are carried out until the forces acting on atoms are below 0.01 eV/Å and the criterion for energy change in electronic step is set to 0.1 meV. To ensure noninteraction of slabs, for all calculations at least 20 Å vacuum space is used. This was proven to be sufficient for the adsorption energy calculation when water molecule is lifted above the surface. Several cases with

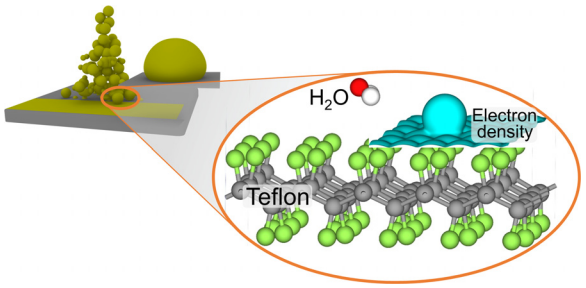

FIG. 1. Schematic illustration of droplet deposition onto a surface during painting shown on the left. The right-hand side image portrays the DFT slab realized in the present study, where water molecule adsorbs hydrophobically on a Teflon surface. The inset in the right-hand side image shows the electron density of the adsorbate. Note: the image on the left is not in scale and presented merely for illustration purposes.

varying slab thickness (i.e., 15 Å, 20 Å, and 25 Å) were considered. The results indicate that the 20 Å thickness is the optimum distance to ensure slabs' noninteraction. Additionally, in order to ensure that the slab size is chosen properly and represents the properties of macroscopic Teflon or parafilm structures, the adsorption energy is calculated for two different slab thicknesses. In general, depending upon the system, the adsorption energy changes by ca. 2% compared to the increase in the slab size by ca. 10%. Thus, the minimum reasonable slab thickness is used as discussed in more detail below. It should be noted that we are aware of other DFT work related to liquid/solid contact surface investigation[30] using PAW-PBE-D3 potential, which could be a subject of future investigations. The adsorption energy of water ($E_{water,ad}$) at the corresponding surface was calculated using the following expression:

$$E_{water,ad} = E_{water} + E_{slab} - E_{water/slab}, \quad (1)$$

where E_{water}, E_{slab}, and $E_{water/slab}$ are the total energy of the isolated water molecule, the energy of the unloaded slab without water

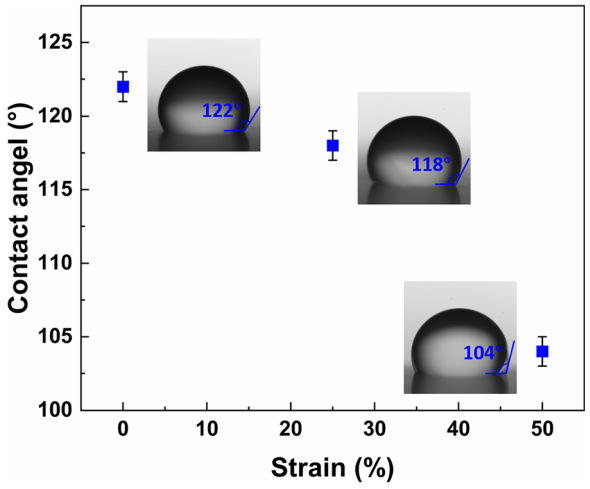

FIG. 2. Equilibrium contact angle of water on Teflon surface at different strains.

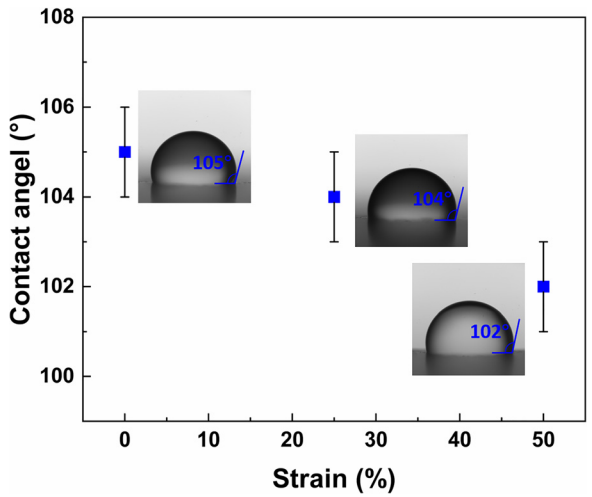

FIG. 3. Equilibrium contact angle of water on parafilm specimen at different strains.

molecule, and the energy of the slab with water molecule adsorbed on top of it.

All Teflon and parafilm surface structures are built using the Atomistic Tool Kit (ATK),[31] which allows one to analyze all possible surfaces, as well as amorphous structure creation. To take into account the influence of the solvent on the adsorption energies of H_2O molecule, we use the implicit solvent (polarized continuum) model[32] as implemented in the VASPsol. Water is considered as a medium with a dielectric constant of 81. In order to create a particular Teflon or parafilm surface in ATK, an elementary repeat unit (C_2F_2 in the case of Teflon and C_2H_2 for parafilm) is repeated in different directions (x and y in the Results and Discussion section) until a reasonably large surface is created. After that, water adsorption energy is calculated and compared for different slab sizes.

Experimental methodology. The static contact angle measurements were conducted on substrates with droplets softly placed on them. The measurements were carried out using imageJ tool. The reported contact angle is the average measured on both sides of the droplet, with an error within ±2°. The influence of gravity on the

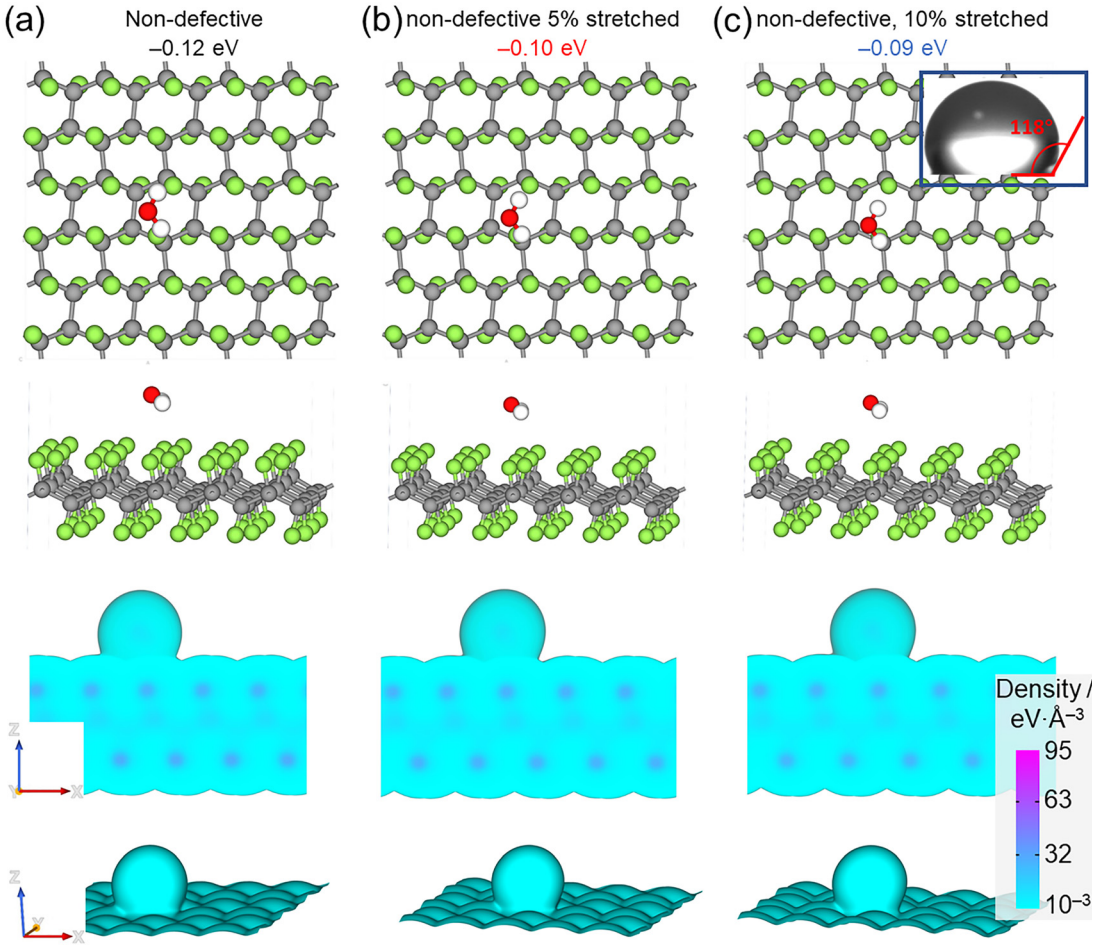

FIG. 4. DFT calculation results of water adsorption on nondefective (a), nondefective, 5% stretched (b) and nondefective, 10% stretched Teflon surface. The first and second rows show atomic configurations of adsorbate on different Teflon surfaces (c), whereas the third and fourth rows depict electron densities: side view (the third row) and top iso-surface (the fourth row) at 0.001 eV/Å. Gray spheres depict carbon atoms, green spheres are fluorine atoms, red spheres are the oxygen atoms, and white spheres denote hydrogen atoms.

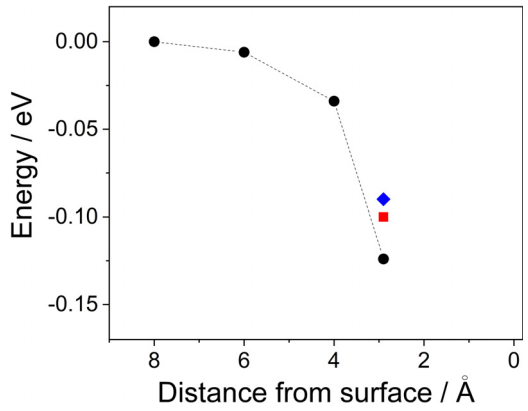

FIG. 5. Water adsorption energy over nondefective surface of Teflon. Solid black circles depict the results for the unstretched surface [Fig. 4(a)], red symbol [Fig. 4(b)] and blue symbol [Fig. 4(c)] correspond to the results for 5% and 10% stretched Teflon surfaces, respectively. Black dashed line serves as an eye guide for water adsorption on the unstretched surface.

contact angle was studied by varying the droplet size (Fig. S4) in supporting information. It was found that the droplet size of 2.5 mm is the optimal size for the static contact angle measurements.

A laboratory syringe supplied water to the 90° bent 30-gauge needle using syringe pump. The average droplet diameters were ∼2.5 mm. Teflon (PTFE) membrane was obtained from McMaster Carr (#6802K16) with a thickness of 0.081 mm. Parafilm M Laboratory Film was obtained from Bemis manufacturer (#PM992). It is referred to as parafilm throughout the text. The thickness of parafilm was 0.127 mm.

III. RESULTS AND DISCUSSION

The primary objective of the present work is to understand water adsorption on Teflon (unstretched and prestretched, cf. Fig. S1 in supplementary material) and parafilm surfaces. For this purpose, the water adsorption energy is calculated at the corresponding surfaces and compared to the experimental data obtained for a static contact angle. In order to make the comparison more realistic in the DFT, the state of the surface has been changed by stretching it or introducing random defects. The results for the Teflon surface are discussed first, followed by the results on water adsorption over the parafilm surface.

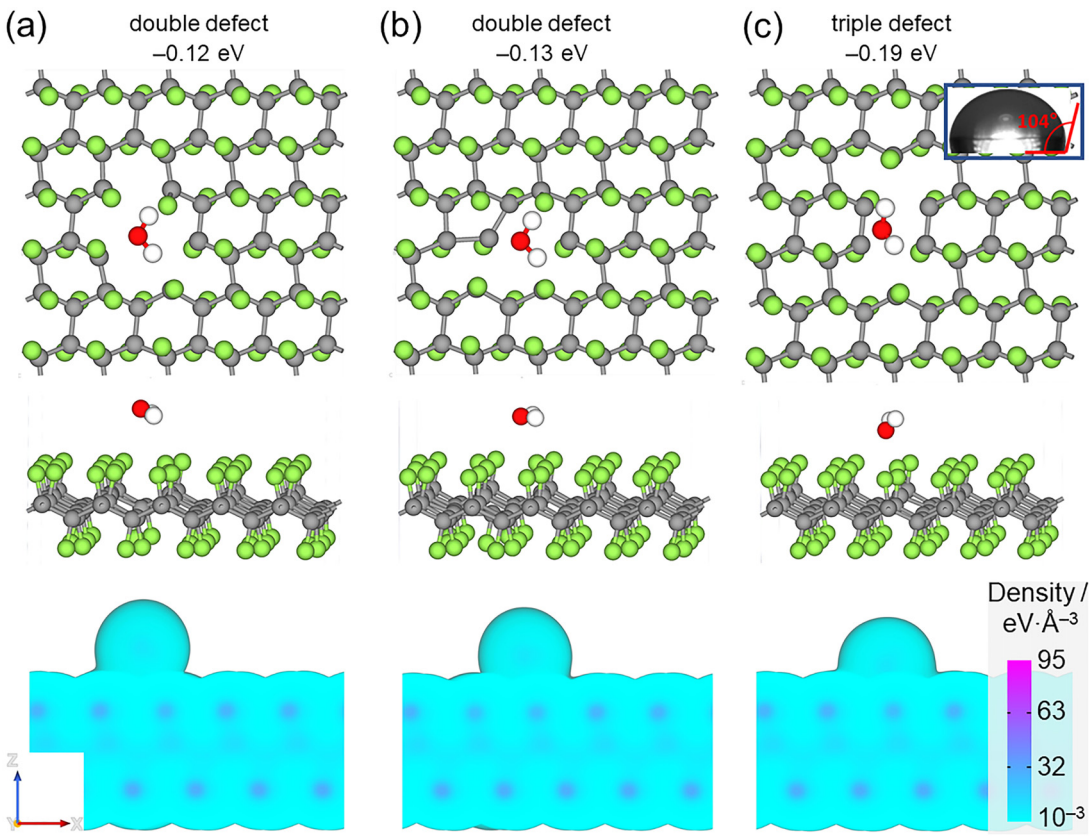

FIG. 6. DFT calculation results for water adsorption on defective Teflon surfaces. The first and second rows depict the atomic configuration of the adsorbate on different defective Teflon surfaces, whereas the third row depicts electron densities corresponding to the side view. The formation of small defects does not lead to a visible change in the adsorption energy. Gray spheres depict carbon atoms (a), green spheres correspond to fluorine atoms (b), red spheres depict oxygen atoms (c), and white spheres denote hydrogen atoms.

A. Contact angle measurement

The contact angles measured for the unstretched and prestretched Teflon specimens are illustrated in Fig. 2. The contact angle of water on the prestretched Teflon revealed a reduction with stretching in comparison to the unstretched Teflon surface.

Similarly, to the Teflon surface, the static contact angle of water droplets on unstretched and prestretched parafilm surfaces was measured, as illustrated in Fig. 3. Stretching of parafilm specimens results in a decrease in the static contact angle from 105° to ∼102°. The comparison of Figs. 2 and 3 reveals that the effect of parafilm stretching on the static contact angle is significantly weaker than that observed for the Teflon surface.

B. DFT results for water adsorption on Teflon surface

The present scanning electron microscopy (SEM) observations (see Fig. S2 in supplementary material) revealed that the Teflon surface facing water droplet contains numerous defects, kinks, and stretching. Obviously, it is impossible to implement such a surface in the DFT calculations; however, it is feasible to mimic the experimentally observed surface by introducing nanostretching and defects. In particular, microscopic stretching as observed in the SEM images would result in the bond stretching between atoms at the nanometer scale. This could be achieved in the DFT by applying strain to the Teflon slab and studying water adsorption on it. On the other hand, microscopic stretching could result in defect formation, where C–F bonds of the Teflon are broken. Such a situation can be reproduced in the DFT simulations by creating random defects in the Teflon surface by removing atoms. In the following, all these scenarios are considered to study water adsorption.

We begin with the DFT calculation results of water adsorption on nondefective unstretched and stretched Teflon surfaces. Figure 4 shows the results of the DFT calculation for nondefective unstretched surface [Fig. 4(a)], nondefective 5% stretched surface [Fig. 4(b)] and nondefective 10% stretched Teflon surface [Fig. 4(c)]. The value of the adsorption energy of water decreases as a result of Teflon stretching by 0.03 eV making the surface more hydrophobic. Using a generally accepted DFT calculation error of 0.01 eV, the change in the adsorption energies should be considered as a trend rather than a quantitative comparison. Analyzing the electron densities in Fig. 4, it can be seen that stretching does not lead to the change of water adsorption nature. The last row in Fig. 4 represents the electron density iso-surface (0.001 eV/Å) illustrating the complexity of water adsorption on the Teflon surface. The present measurements demonstrated that stretching of the Teflon surface results in change of the static contact angle toward more hydrophilic (the inset in the upper right corner in Fig. 4). On the first glance, these results contradict the DFT calculation results presented in Fig. 4, where Teflon stretching leads to more hydrophobic surface as a result of stretching. However, the macroscopic stretching performed in the experiments is not the same as the atomic stretching done in the DFT calculations. The stretching of the surface in the DFT calculations is performed by elongating bonds between atoms, whereas in the experiment the stretching is realized between separate macroscopic parts of Teflon chains. This macroscopic stretching provokes the formation of different kinds of defects and microvalleys, where water can potentially become trapped and results in a more hydrophilic surface. This scenario has been studied too and the results are presented below.

Following the results for a nonstretched Teflon surface presented in Fig. 4, we have calculated the adsorption energies of water as a function of a distance from the Teflon surface. Figure 5 presents the adsorption energy values as a function of the distance from the surface. The equilibrium adsorption distance between water and the unstretched Teflon is 2.9 Å corresponding to the left-hand side column in Fig. 4 with the adsorption energy of −0.12 eV (cf. solid black symbols in Fig. 5). The red and blue colored symbols in Fig. 5 depict the results for water adsorption on the 5% and 10% stretched Teflon surfaces, respectively. The stretching of the Teflon surface leads to a weaker adsorption of water. The results presented in Fig. 5 indicate that water interaction (via weak van der Waals forces) with the Teflon surface

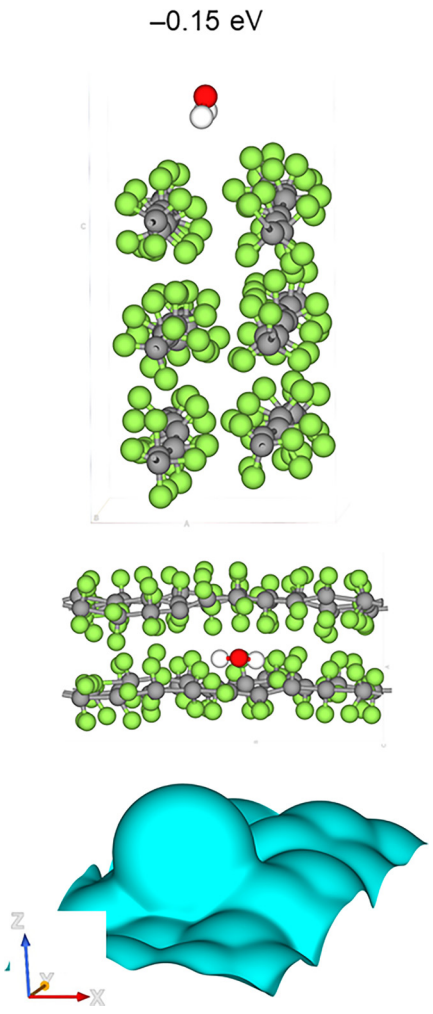

FIG. 7. DFT calculation results of water adsorption on amorphous Teflon surface. The top and middle images depict atomic configuration of the adsorbate on amorphous Teflon surfaces (side and top view). The bottom image shows the electron density surface at 0.001 eV/Å. Gray spheres depict carbon atoms, green spheres—fluorine atoms, red spheres—the oxygen atoms, and white spheres denote hydrogen atoms.

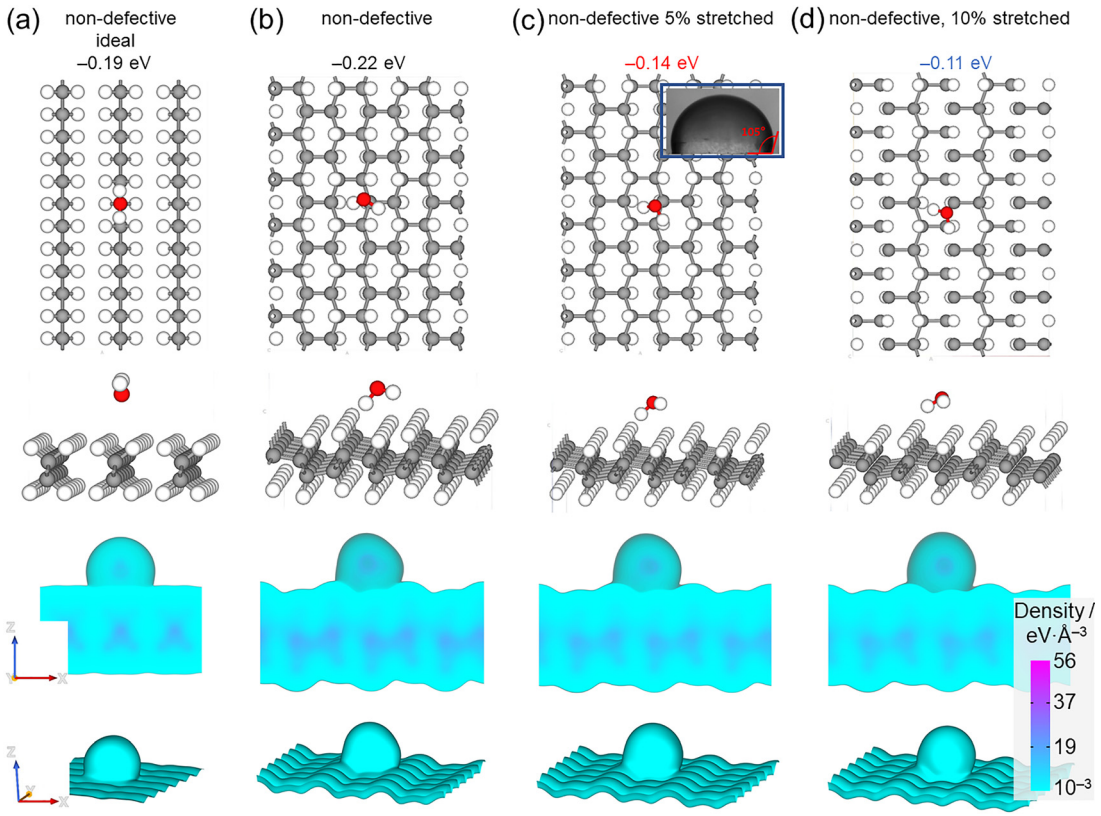

FIG. 8. DFT calculation results of water adsorption on nondefective ideal (a), nondefective (b), nondefective, 5% stretched (c) and nondefective, 10% stretched (d) parafilm surface. The first and second rows from the top show atomic configuration of the adsorbate on different paraffin surfaces, whereas the third and fourth rows depict electron densities: the side view (the third row) and the top iso-surface (the fourth row). The iso-surface scale is chosen as 0.001 eV/Å^3. Gray spheres depict carbon atoms, red spheres—the oxygen atoms, and white spheres denote hydrogen atoms.

already begins at the distance of ca. 6 Å despite hydrophobicity of Teflon.

We have further calculated water adsorption on defective unstretched Teflon surface. Figure 6 depicts the surface structures (the first and second rows) together with the electron densities (the last row) of water adsorbed on the defective Teflon surface. The introduction of small single and double defects does not significantly change the adsorbate structure or the adsorption energies. The left-hand side and middle columns show the results for these water adsorption cases, where the predicted adsorption energy of water eventually does not change within the error of the DFT calculations. The results shown in Fig. 6(c) are related to triple defective site which results in a visible increase in the adsorption energy, which makes the Teflon surface hydrophilic as revealed by electron density. Comparing these results to the experimental data (the inset in the upper right corner in Fig. 6), we may conclude that macroscopic stretching in the experiment results in the creation of defective sites or nanovalleys, where water can be trapped.

The SEM images (Fig. S2 in supplementary material) reveal significant distortions of Teflon surface, which occur as a result of stretching or sample preparation itself. For that reason, in the

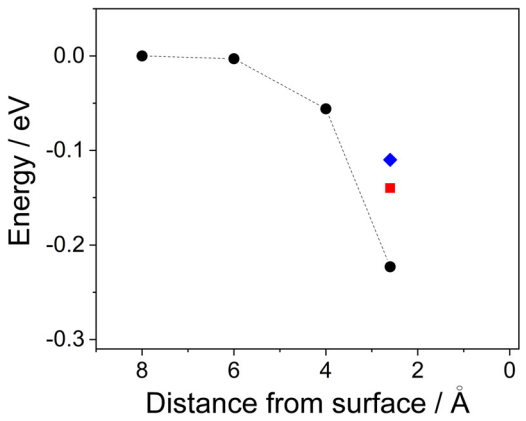

FIG. 9. Water adsorption energy over parafilm nondefective surface. Solid black circles [cf. Fig. 8(b)] depict results for the unstretched surface, whereas red [cf. Fig. 8(c)] and blue [cf. Fig. 8(d)] symbols depict the results for the 5% and 10% stretched parafilm, respectively.

calculations, an amorphous Teflon surface was created and water adsorption energy was calculated. Figure 7 shows water adsorption configuration over the amorphous structure of Teflon together with the corresponding electron density iso-surface at 0.001 eV/Å. Figure 7 reveals that water adsorption on the amorphous structure is more similar to hydrophilic situation judging from the adsorption energy (−0.15 eV) and the electron density profile. This indicates that the amorphization of Teflon surface may lead to hydrophilicity facilitated by the formation of nanovalleys where water is trapped.

Relating the above-presented DFT results to the present experimental data for the static contact angle and the corresponding SEM Teflon surface images, one can conclude that macroscopic stretching results in nanovalleys, where water adsorbs stronger, facilitating surface hydrophilicity. In particular, such a trend is observed comparing the results shown in Fig. 4(a) to the results depicted in Fig. 4(c). The 5% stretching produces more defective sites, where water binds stronger than on nondefective sites. From a fundamental standpoint, the Teflon surface does not become hydrophilic as a result of stretching but rather changes the surface geometry resulting in water trapping. This is supported by the fact that macroscopic stretching does not change an intensive property of Teflon. Moreover, the present DFT findings stay in good agreement with the macroscopic Wenzel model. According to the latter, surface roughness facilitates wettability (i.e., hydrophilicity) in comparison to the corresponding smooth surface. The results presented in Fig. 6 indicate that the introduction of defective sites (chemically heterogeneous state) makes the surface more hydrophilic. On the other hand, a simple stretching of the hydrophobic surface as shown in Fig. 4 results in a higher hydrophobicity, in agreement with the Wenzel model.[33]

Based upon these results, we can conclude that experimental effort should be focused on achieving a particular stretching percentage that is sufficient to withhold macroscopic characteristics of Teflon and simultaneously produce defective sites for better water adsorption.

C. DFT results for water interaction with parafilm surface

Next, we present the DFT results for water adsorption on parafilm surface (cf. Fig. 3). Similarly, to the simulations of Teflon surface, two sets of calculations for nondefective parafilm surface and a defective parafilm surface were performed. The nondefective parafilm

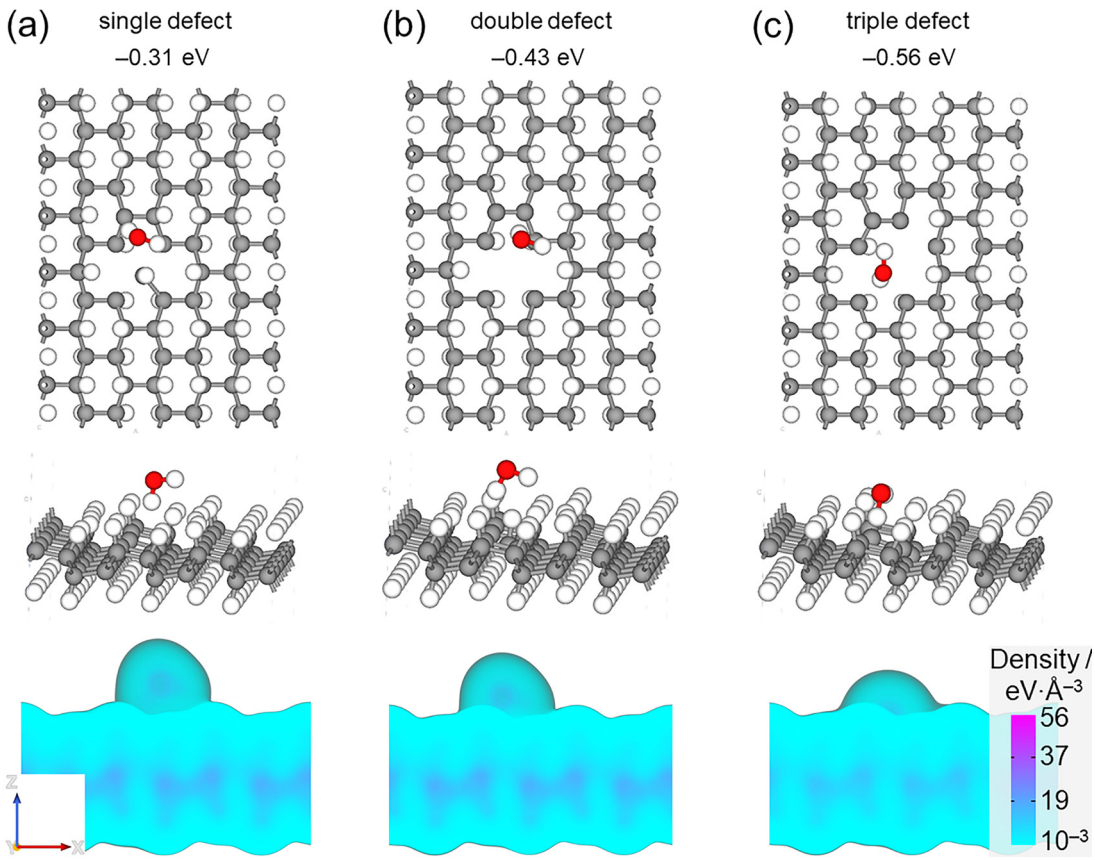

FIG. 10. DFT calculation results of water adsorption on single defective (a), double defective (b) and triple defective (c) parafilm surfaces. The first and second rows depict the atomic configuration of the adsorbate on different defective parafilm surfaces. The third row depicts electron densities shown in side view. These results indicate that defective parafilm surface is hydrophilic in comparison to the hydrophobic ideal surface. Gray spheres depict carbon atoms, red spheres—the oxygen atoms, and white spheres denote hydrogen atoms.

surface also includes the amorphous structure to better understand water interaction.

Figure 8 presents the results of the DFT calculations of water adsorption on the unstretched and stretched nondefective parafilm surfaces. Two unstretched surfaces were considered: an ideal parafilm surface [Fig. 8(a)] and a more realistic one with steps and kinks [Fig. 8(b)]. The adsorption energy on both surfaces revealed very similar values (−0.19 eV and −0.22 eV, respectively) indicating that small distortions on a surface do not influence water adsorption energy. The stretching of the surface to 5% and 10% (the last two columns in Fig. 8) results in decrease in the magnitude of the adsorption energy making the parafilm surface more hydrophobic similarly to the case of Teflon (cf. Fig. 4). Comparing the results on water adsorption on Teflon and parafilm nondefective stretched surfaces, we may conclude that the macroscopic stretching performed in the experiments not only leads to bond elongation but also to creation of numerous defects and kinks. These defects facilitate water trapping, promoting hydrophilicity. On the other hand, our DFT calculation results reveal an important aspect of hydrophobic surface creation. In order to create a highly hydrophobic surface experimentally, a uniform stretching should be performed without bond breaking.

Similarly to Teflon surface, the water adsorption energy on the parafilm surface was predicted as a function of the distance from the surface (Fig. 9). The equilibrium distance is 2.5 Å with the adsorption energy of −0.22 eV [the adsorption configuration is shown in Fig. 8(b)]. As water molecule is moved away from the surface, the interaction weakens, leading to the noninteraction at ∼8 Å. Two additional red and blue points in Fig. 9 describe 5% and 10% stretching of the parafilm surface [Figs. 8(c) and 8(d)]. These results reveal a similar trend as the one predicted for water adsorption on Teflon surface. However, water adsorbs stronger on the parafilm surface in comparison to the similar Teflon surface state.

Water adsorption on defective parafilm surface has been studied by creating single, double, and triple defects, as shown in Fig. 10. Surprisingly, formation of a single-type defect results in a significant water adsorption strength (the adsorption energy of −0.31 eV in comparison to the value for the nondefective surface of −0.22 eV), which is the opposite trend to the Teflon surface (see Fig. 6). Accordingly, the double and triple-type defective sites adsorb water even stronger, resulting in a highly hydrophilic parafilm surface. These DFT results indicate that macroscopic stretching produces both elongation of bonds as well as nanovalleys, where water can adsorb stronger. We do not observe any change in the nature of water adsorption on parafilm surface in the experiments with the static contact angle measurement even for the strain as high as 50%. This could be related to the type of parafilm surface employed in the measurements and should be explored in more detail in future.

Next, we have calculated water adsorption on the amorphous parafilm surface. Figure 11 depicts these results revealing that the amorphization tends to increase water adsorption strength, suggesting the presence of amorphous-like structure resulting from the macroscopic stretching in the present experiments.

IV. SUMMARY AND CONCLUSIONS

The DFT calculations are performed to reveal the dominant water adsorption sites, energetics, and the electron density profiles on Teflon and parafilm surfaces. Several surface states such as nonstretched, stretched, nondefective, defective, and amorphous are considered for water adsorption. It is revealed that stretching of nondefective surface leads to weaker water adsorption compared to an unstretched surface. Accordingly, such a stretching makes the surface more hydrophobic as revealed by the electron density profile. The introduction of random defects into Teflon and parafilm surfaces results in an increase in the water adsorption energy, even leading to hydrophilicity in some cases. This is in good agreement with the present experimental results for prestretched Teflon and parafilm samples, where stretching not only elongates interatomic bonds but also changes the surface roughness. Overall, our combined DFT and experimental results for the static contact angle agree well with the macroscopic Wenzel model trend.

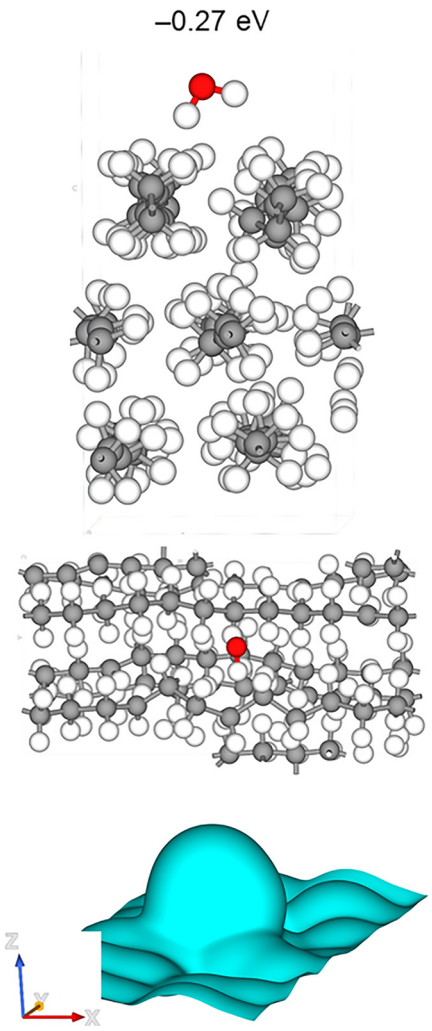

FIG. 11. DFT calculation results of water adsorption on amorphous parafilm surface. The first and second images from the top depict the atomic configuration of the adsorbate on the amorphous parafilm surfaces (the side and top views, respectively). The third image depicts the electron density surface at 0.001 eV/Å. Gray spheres depict carbon atoms, red spheres—the oxygen atoms, and white spheres denote hydrogen atoms.

It should be emphasized that there is certainly no guarantee of universal applicability of the present DFT results to macroscopic treatment of hydrophobic surfaces. However, the DFT results facilitate significant qualitative insights into fundamental processes during water interaction with Teflon and parafilm surfaces. Moreover, if more comprehensive, perhaps high-resolution transmission electron microscopy (HRTEM), imaging of Teflon and parafilm surfaces at the nanoscale would become available, some additional DFT calculations might certainly be reconsidered based upon a new morphological information. Nevertheless, the present *ab initio* modeling results seem to provide a reasonable qualitative representation of the present macroscopic experimental data and shed light on important aspects of water interaction with hydrophobic surfaces.

SUPPLEMENTARY MATERIAL

See the supplementary material for details of experimental measurements of the static contact angle as well as the scanning electron microscopy (SEM) imaging, and presents the corresponding results.

ACKNOWLEDGMENTS

The authors acknowledge the financial support from the National Science Foundation Award No. CBET-1906497. In addition, we would like to acknowledge the Advanced Cyberinfrastructure for Education and Research (ACER) group at The University of Illinois at Chicago (https://acer.uic.edu) for providing HPC resources that have contributed to the research results reported in this paper.

DATA AVAILABILITY

The data that support the findings of this study are available within the article and its supplementary material.

REFERENCES

[1]P. K. Tyagi, R. Kumar, and P. K. Mondal, Phys. Fluids **32**, 121301 (2020).
[2]A. L. Yarin, Annu. Rev. Fluid Mech. **38**, 159 (2006).
[3]A. L. Yarin, I. V. Roisman, and C. Tropea, *Collision Phenomena in Liquids and Solids* (Cambridge University Press, Cambridge, 2017).
[4]S. Yun and G. Lim, J. Fluid Mech. **752**, 266 (2014).
[5]R. Rioboo, M. Marengo, and C. Tropea, Exp. Fluids **33**, 112 (2002).
[6]J. Plog, J. M. Löwe, Y. Jiang, Y. Pan, and A. L. Yarin, Langmuir **35**, 11023 (2019).
[7]S. Ding, X. Liu, X. Wu, and X. Zhang, Phys. Fluids **32**, 102106 (2020).
[8]R. Rioboo, C. Tropea, and M. Marengo, At. Sprays **11**, 155 (2001).
[9]S. A. Banitabaei and A. Amirfazli, Phys. Fluids **29**, 062111 (2017).
[10]Y. Cheng, J. Li, J. Xu, and Y. Shen, Walls **33**, 032001 (2021).
[11]J. Hao, Phys. Fluids **29**, 122105 (2017).
[12]M. Moradi, M. H. Rahimian, and S. F. Chini, Phys. Fluids **32**, 062110 (2020).
[13]A. P. Hughes, U. Thiele, and A. J. Archer, J. Chem. Phys. **142**, 074702 (2015).
[14]J. Di, Z. Yang, and Y. Duan, AIP Adv. **9**, 125105 (2019).
[15]M. Areshi, D. Tseluiko, and A. J. Archer, Phys. Rev. Fluids **4**, 104006 (2019).
[16]K. Yokoi, D. Vadillo, J. Hinch, and I. Hutchings, Phys. Fluids **21**, 072102 (2009).
[17]Š. Šikalo, H. D. Wilhelm, I. V. Roisman, S. Jakirlić, and C. Tropea, Phys. Fluids **17**, 062103 (2005).
[18]V. Yurkiv, A. L. Yarin, and F. Mashayek, Langmuir **34**, 10169 (2018).
[19]J. H. Weijs, A. Marchand, B. Andreotti, D. Lohse, and J. H. Snoeijer, Phys. Fluids **23**, 022001 (2011).
[20]J. Guo, S. Zou, S. Lin, B. Zhao, X. Deng, and L. Chen, Phys. Fluids **32**, 122112 (2020).
[21]E. Sauer and J. Gross, Ind. Eng. Chem. Res. **56**, 4119 (2017).
[22]E. Sauer, A. Terzis, M. Theiss, B. Weigand, and J. Gross, Langmuir **34**, 12519 (2018).
[23]J. Gross, J. Chem. Phys. **131**, 204705 (2009).
[24]P. Rehner and J. Gross, J. Chem. Phys. **148**, 164703 (2018).
[25]A. P. Hughes, U. Thiele, and A. J. Archer, J. Chem. Phys. **146**, 064705 (2017).
[26]A. P. Hughes, U. Thiele, and A. J. Archer, Am. J. Phys. **82**, 1119 (2014).
[27]M. Brownell and A. K. Nair, Phys. Chem. Chem. Phys. **21**, 490 (2019).
[28]J. Klimes, D. R. Bowler, and A. Michaelides, Phys. Rev. B **83**, 195131 (2011).
[29]J. Klimes, D. R. Bowler, and A. Michaelides, J. Phys.: Condens. Matter **22**, 022201 (2010).
[30]J. Li and F. Wang, J. Chem. Phys. **146**, 054702 (2017).
[31]Atomistix Toolkit Version 2017.2, Synopsys QuantumWise A/S (2017).
[32]K. Mathew, R. Sundararaman, K. Letchworth-Weaver, T. A. Arias, and R. G. Hennig, J. Chem. Phys. **140**, 084106 (2014).
[33]S. A. Egorov and K. Binder, J. Chem. Phys. **152**, 194707 (2020).